Charge-Governed Solvation Behaviour of Novel AMPs

Peicho Petkov, Rositsa Marinova, Leandar Litov, Elena Lilkova, Frédéric Allemand, Assia Mouhand, Aurélien Thureau, Nathalie Sibille, Nevena Ilieva

Charge-Governed Solvation Behaviour of Novel AMPs

Peicho Petkov[1], Rositsa Marinova[*1], Leandar Litov[1], Elena Lilkova[2], Frédéric Allemand[3], Assia Mouhand[3], Aurélien Thureau[4], Nathalie Sibille[3], and Nevena Ilieva[2,5]

[1]Faculty of Physics, Sofia University "St. Kliment Ohridski", Bulgaria
[2]Institute of Information and Communication Technologies at the Bulgarian Academy of Sciences, Bulgaria
[3]Centre de Biologie Structurale (CBS), CNRS, Univ. Montpellier, France
[4]HélioBio Section, Synchrotron SOLEIL, L'Orme des Merisiers, France
[5]Institute of Mathematics and Informatics at the Bulgarian Academy of Sciences, Bulgaria

Abstract. *Antimicrobial peptides (AMPs) are regarded as a promising alternative to conventional antimicrobials, but their mechanism of action is not completely understood. Using long-scale molecular dynamics simulations, we investigate the behavior of two newly isolated AMPs from the Helix aspersa mucus fraction with molecular weight (MW) below 3 kDa in mono- and multicomponent solutions, prior to their engagement with the pathogenic membrane. In both instances, the peptide monomers form clusters consisting of a non-polar hydrophobic nucleus surrounded by charged and polar residues exposed to the solvent. We consider the so-formed structures to be the ideal transport and coalescence system – locking the hydrophobic uncharged residues in the cluster core prevents interaction with the eukaryotic membranes, while solvent exposed charged residues enable electrostatic interaction with the bacterial surface. In addition, the amphiphilic structure of the aggregates promotes peptide folding, which increases the local concentration of AMPs delivered to the target membrane in a functionally active conformation.*

*Correspondence: rosie.marinova@gmail.com

1 Introduction

Antimicrobial peptides (AMPs) are naturally occurring molecules that are released by almost all forms of life as part of the innate immune response of the host [57, 3]. They are small proteins that consist of less than 100 amino acid residues. AMPs are structurally diverse, adopting α-helical, β-sheet, mixed, extended or cyclic conformations [16]. Usually, AMPs are cationic, with a net charge ranging from +2e to +9e, and have an amphiphilic nature [25, 56]. AMPs display fast and effective antimicrobial activity against a broad spectrum of both Gram-positive and Gram-negative bacteria, fungi, parasites, some viruses and even cancer cells [3, 18, 56, 5]. Notably, so far bacteria have not succeeded to develop efficient resistance against their action [17, 35, 32, 7]. All this makes them a promising alternative to the conventional antimicrobial agents in view of the alarmingly growing number of multi-drug resistant bacterial strains.

Despite their different structure and functions, the interaction of AMPs with the pathogens usually leads to cell lysis, either by disrupting membrane integrity and function, or by translocation and inhibition of important cellular processes and biosynthesis of macromolecules [35, 19]. Therefore, the development of bacterial resistance to AMPs requires not just single modifications of

Table 1: Novel peptides, isolated from the mucus extract of the garden snail Helix aspersa.

Peptide	Sequence	Charge	Molecular weight [kDa]
p1	KVKDNQWRP	+2	1.17
p2	VNVVGGGGGIVGGGIGGGGM	0	1.57

certain receptors, as in the case of conventional antibiotics, but a complete change of the properties of the membrane, which is difficult to achieve. Thus, due to their unique physicochemical properties, broad-spectrum activity, selectivity and low probability of developing resistance to them, AMPs arise as a promising therapeutic alternative to the conventional small-molecule antibiotics [17, 32, 7].

The proper understanding of the antimicrobial action of AMPs is still an open problem [38, 45]. In general, their bactericidal activity results from their interaction with the target bacterial membrane [19, 45]. However, multiple aspects of this interaction are still controversial, including which is the AMPs biologically active secondary structure, how and when do they adopt it, and what is the AMPs behavior in the bodily liquids prior to attacking the target membrane.

Peptides isolated from mollusks and arthropods exhibit a broad spectrum of antimicrobial activity against various Gram-positive and Gram-negative bacterial strains [59, 29, 12, 11, 43, 58]. Recently, a series of novel proline- and glycine-rich putative AMPs have been identified from the mucus of the garden snail *Helix aspersa* [53, 13, 24, 14]. The snail mucus, known for its antibacterial, antiviral and fungicidal properties, is a complex mixture of a variety of peptides, carbohydrates and other low-molecular weight compounds [53, 13, 14]. Revealing the specific role of the different components of this mixture will bring us closer to understanding the antimicrobial action of these natural substances and will help design, on this basis, therapeutics with tailored activity. In the present study, we focus on exploring the behaviour of two newly identified AMPs from the mucus fraction with MW ¡ 3 kDa — one with a high (positive) charge and the other neutral — prior to their engagement with the pathogenic membrane. We report our findings, based on long-scale molecular dynamics (MD) simulations of mono- and multicomponent peptide solutions of these two novel AMPs, supported by structural studies by means of CD, SEC-MALS, and SAXS measurements.

2 Materials and Methods

2.1 Input structures

The primary sequences of the investigated peptides [24] are presented in Table 1. They are newly isolated, so there is no structural data about them. For developing 3D molecular models as input structures for the subsequent computational studies, the two sequences were generated in completely extended conformations and then subjected to 1 μs folding simulations using molecular dynamics (MD). The simulation protocol is described in section 2.2. The obtained conformations were analysed to define input structures for the simulations of both peptides in concentrated mono- and multicomponent solutions.

The selected equilibrated peptide monomer structures were used to build solutions of multiple peptides in a cubic simulation box. The initial distance between two peptides was 5 nm. 27 monomers were used for the monocomponent solutions, and 25 monomers of p1 and 10 monomers of p2 (ratio 2.5:1) were used in the mixture. Another series of simulations was performed for all three systems at a concentration of 10 mg/mL, the third one being studied in this setup also at a composition ratio 1:1. The resulting simulation boxes and concentrations are given in Table 2.

2.2 MD simulation protocol

All simulations were performed with the MD simulation package GROMACS 2016.8 [2]. The CHARMM36 force field was used for parameterization of the peptides [34], in combination with the modified TIP3PS water model for the solvent [33]. The peptides were solvated in cubic boxes with a minimal distance to the box walls of

Table 2: Simulations setup.

Peptide type	# Monomers	Box dimensions [Å^3]	Concentration [mg/mL]
p1	27	$80.7 \times 89 \times 130.7$	55.8
p2	27	$110.7 \times 114.3 \times 123.8$	44.9
p1	27	$173.7 \times 173.7 \times 173.7$	10.0
p2	27	$191.6 \times 191.6 \times 191.6$	10.0
p1+p2	25+10	$163.31 \times 163.31 \times 163.31$	11.1 & 6.0

1.2 nm under periodic boundary conditions. Sodium and chlorine ions with a 0.15 mol/l concentration were added to all systems to neutralize their net charge and to ensure physiological salinity of the solution. The systems were energy minimized using the steepest descent with a maximum force tolerance of 10 kJ/(mol nm), followed by short 50 ps position-restraint simulations to equilibrate the solvent. Then 10 ns isothermal-isobaric simulations were performed, in which the temperature was gradually increased to 310 K using v-rescale thermostat [6] with a coupling constant of 0.1 ps and pressure was equilibrated at 1 atm using Parrinello-Rahman barostat [39, 40] with a coupling constant of 2 ps.

The production MD simulations were also performed in the NPT-ensemble using the same thermo- and barostat parameters. The leapfrog integrator [21] was used with a time-step of 2 fs, while constraints were imposed on bonds between heavy atoms and hydrogens using the PLINCS algorithm [20]. Van der Waals interactions were smoothly switched off from a distance of 1.0 nm and truncated at 1.2 nm. Electrostatic interactions were treated using the smooth PME method [15] with a direct PME cut-off of 1.2 nm. Neighbour lists were constructed every 10 ps. Each production simulation had a duration of 2 μs. Trajectory frames were recorded every 100 ps.

2.3 Umbrella sampling simulations

To estimate the dissociation free energy of charged peptides from the peptide aggregate, we used a series of umbrella sampling (US) simulations. The reaction coordinates ξ_1, ξ_2, ξ_3 for three simulation series were defined as the center-of-mass (COM) distance between the aggregate and the three most solvent-exposed p1 peptides that participate in it.

The simulation protocol, developed by Lemkul et al. [28] was employed for the calculation of the potential of mean force (PMF). Firstly, steered MD (SMD) simulations were performed using the GROMACS pull code in order to generate configurations along each of the chosen collective variables (CVs), whereas the aggregate heavy atoms were kept constrained and the chosen peptide was pulled at a rate 0.01 nm/ps using a harmonic potential with a spring-force constant of 1000 kJ/(mol nm^2). SMD trajectory frames were written every ps. Then configurations from the SMD trajectories were selected using a 0.1 nm window. The selected configurations served as starting configurations for the series of 50 US simulations for each CV. 100 ps NPT equilibration simulations were run in each US window and then conformations were collected for 1 ns.

2.4 Synthetic data analysis

The MD trajectories were post-processed and analysed using the standard GROMACS post-processing and analysis tools. Secondary structure was assigned by the DSSP algorithm [26]. All structural figures were generated by the visualisation and manipulation package VMD [23]. The US PMF along each collective variable was obtained using the Weighted Histogram Analysis Method (WHAM) [27], as implemented in GROMACS [22]. The Bayesian bootstrap of complete histograms method [22] with 200 bootstraps was used for error estimation of the calculated PMF.

2.5 Far-UV-Circular Dichroism measurement and analysis

Measurements were realized with a Chirascan V4.5 from Applied PhotophysicsTM at 23°C. Spectra were scanned from 190 to 260 nm with an increment of 0.5 nm and an integration time of 1 s, the pathlength was 10 mm and the bandwidth was 0.5 nm. 350 μL solutions of p1 and p2 peptides were prepared at a concentration of 0.1 mg/mL in 50 mM BisTris pH 6.7, 50 mM NaCl buffer. All peptides were loaded in a quartz cuvette with a light path of 1 mm and the buffer scan signal was subtracted from the corresponding sample scan. Secondary structure analyses were performed using DICHROWEB [37], a web interface, calculating protein secondary structure from circular dichroism spectroscopic data. Deconvolutions were done with the CONTINLL algorithm [44] using reference data set 4 [47]. The results were evaluated based on NRMSD – a fit parameter, which is a measure of the difference between the experimental ellipticities and the ellipticities of the back-calculated spectra for the derived structure. It is defined as

$$NRMSD = \sum \sqrt{(\theta_{exp} - \theta_{cal})^2 / \theta_{exp}^2},$$

summed over all wavelengths.

For higher concentrated p1 and p2 samples (at 5.5 mg/mL and 5.7 mg/mL respectively), circular dichroism (SRCD) was performed on the DISCO beamline at the synchrotron SOLEIL (Saint-Aubin, France). Spectra were recorded at 25 °C with an integration time of 2 s and a bandwidth of 1 nm with a resolution of 1 nm.

2.6 Size-Exclusion Chromatography-Multi Angle Light Scattering (SEC-MALS)

The Size-Exclusion Chromatography-Multi Angle Light Scattering (SEC-MALS) experiment was performed at 25°C using a Superdex Peptide 10/300 GL column (Cytiva^{TM}) connected to a miniDAWN-TREOS light scattering detector and an Optilab T-rEX differential refractive index detector (Wyatt Technology, Santa Barbara, CA). The column was equilibrated with 0.1 μm filtered 50 mM BisTris pH 6.7, 50 mM NaCl buffer and the SEC-MALS system was calibrated with a sample of Bovine Serum Albumin (BSA) at 1 mg/mL. Samples of 30 μL of p1 and p2 at 10 mg/mL were injected at 0.5 mL/min. Data acquisition and analyses were performed using the ASTRA software (Wyatt^{TM}).

2.7 Small-angle X-ray scattering (SAXS) measurement and analysis

The SAXS data for p1 and p2 was collected at the SWING beamline at the SOLEIL synchrotron, France, equipped with an Eiger 4M detector with a sample-to-detector distance of 2 m [51]. Samples were measured at 15°C and at three concentrations, 2.5 mg/mL, 5 mg/mL and 10 mg/mL, for all peptides, in 50 mM BisTris pH 6.7, 50 mM NaCl and 2 mM DTT buffer. The intensity was measured as a function of the magnitude of the scattering vector, q, according to [4]:

$$q = 4\pi \sin\theta\lambda$$

where θ is the scattering angle and λ is the X-ray wavelength. The scattering profiles covered a momentum transfer range of 0.004 ¡ s ¡ 0.56 Å^{-1}. Data was processed using FOXTROT (SWING beamline software) to automatically select frames corresponding to buffer and sample, and to perform buffer subtraction. The subtracted SAXS curves were analyzed using the Primus tool from ATSAS software package.

3 Results

3.1 Peptide monomers in water

The investigated peptides are newly isolated and defined through their amino acid sequences. In the absence of 3D-structure data, folding simulations with a duration of 0.5 $|mu$s, resp. 1 μs were undertaken for both from a completely extended conformation. For the nonapeptide it was to be expected to remain largely unstructured, while with its 20 residues p2 might have formed a specific fold. The simulations did not reveal a preferred conformation for any of the two peptides. Throughout the p2 simulation, a beta bridge was formed occasionally between Val^3 and Ile^{10} (Fig. 1a), but as seen in Fig. 1b, on average only 2.8 residues adopted a structured (helix, extended-beta, bridge or turn) conformation. Individual occupancies of the various secondary structures were presented in Suppl. Fig. S1.

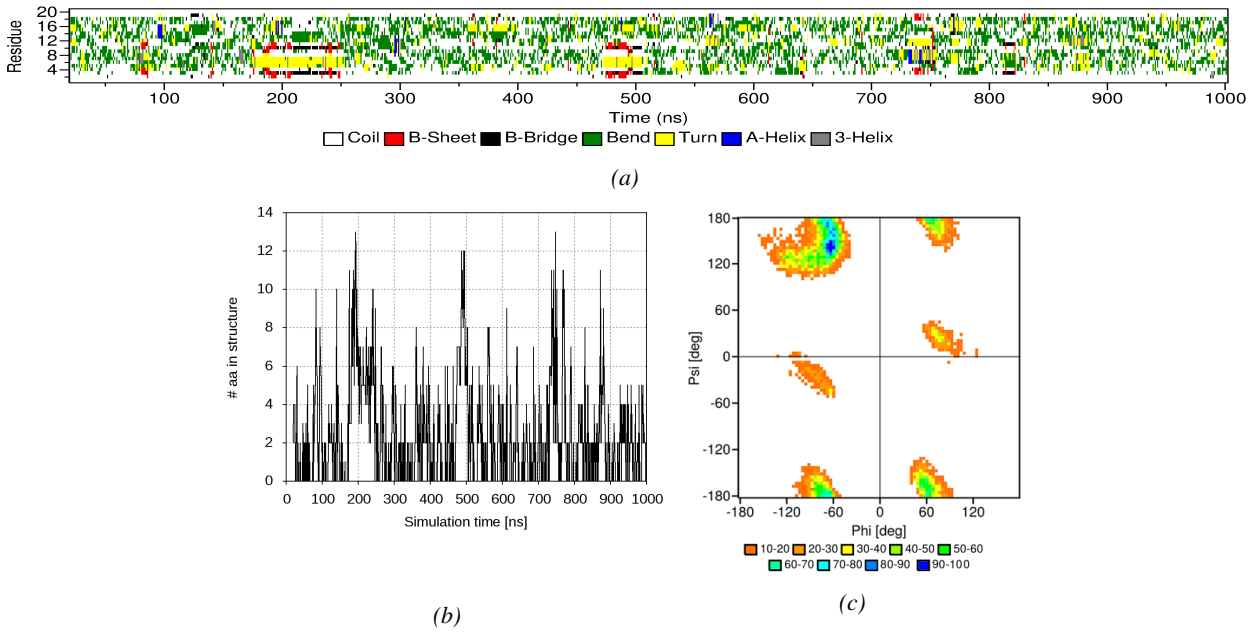

Figure 1: a Secondary structure; b Number of amino acid residues in any secondary structure element; c Ramachandran plot of the p2 monomer in water.

The lack of secondary structure and, consequently, any defined tertiary fold is due to the high glycine content of the p2 peptide. Out of the 20 amino acid residues, 12 are glycines. The occupancy in the Ramachandran plot (Fig. 1c) very closely resembles the all-glycine (ϕ, ψ)-backbone angles distribution in [31].

Since both peptides did not fold to any well-defined structure, the subsequent simulations were started from a randomly chosen conformation from the folding simulations (Suppl. Fig. S2).

3.2 Mono-component peptide solutions

In order to study the behavior of AMPs after their secretion in the bodily fluids (in this case snail mucus) and prior to their interaction with the pathogenic membrane, we performed 1 μs MD simulations of mono-component solutions of 27 p1 or p2 peptides placed on a rectangular lattice with a distance of 5 nm between the monomers.

In both simulations the peptides quickly started to form dimers, trimers and larger oligomers. This was especially true for the p2 solution, where within the first 20 ns of the trajectory all 27 peptides clumped together in one large aggregate. This behaviour is displayed by the blue curve in Fig. 2, which shows the number of monomers, participating in the largest aggregate in the simulation box.

The p2 peptide is very hydrophobic — in addition to the 12 non-polar glycines, it contains four valines, two isoleucines and a methionine, that are among the most hydrophobic amino acids, and just one polar residue, an asparagine. Obviously, the aggregation process of the p2 peptides is entirely governed by the hydrophobic effect.

Interestingly, the p1 peptide, having a more classical AMP sequence and containing both hydrophobic and polar or charged residues, also aggregated. However, in this case the size of the cluster was determined by the balancing out of the hydrophobic effect and the electrostatic repulsion of the charged amino acids. On average, the largest p1 aggregates contained 7 monomers (red curve in Fig. 2). The largest clusters in the two mono-component simulations are shown in Fig. 3. In addition to their size, the two aggregate structures also differ in their den-

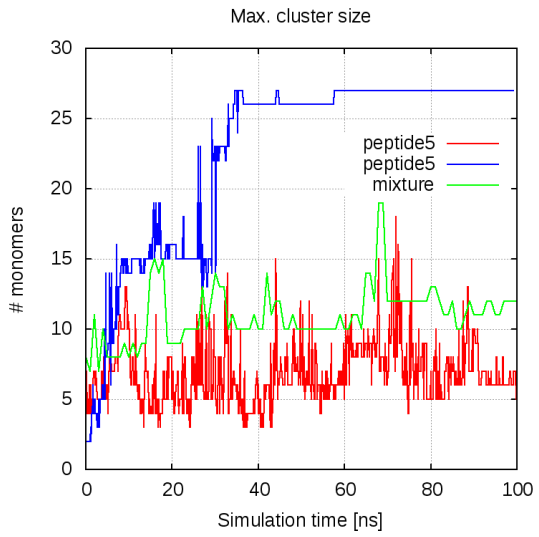

Figure 2: Maximal cluster size for the three peptide solution simulations

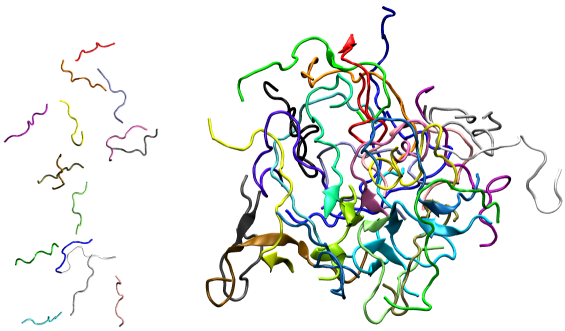

(a) *(b)*

Figure 3: Largest aggregates in the mono-component a p1 and b p2 peptide solution simulation. Different colours correspond to different peptide monomers.

sity. The p1 cluster is fairly loose, with large distance between the monomers, whereas the p2 cluster is very tightly packed.

Upon aggregation, some of the peptides form stable inter-chain secondary structure elements. This tendency is observed both for the short highly charged p1 peptide (Fig. 4a) and for the longer neutral hydrophobic p2 peptide (Fig. 4b). On average, within the last 150 ns of the p1 solution simulation, 17 amino acid residues are in a structured conformation, mainly participating in turns, but also β-bridges and even some β-sheets (Suppl. Fig. S2). The increase in structured residues for the p2 mono-component solution is mainly due to the formation of β-bridges and β-sheets (Suppl. Fig. S3). In the last 150 ns of the p2 solution simulation the average number of the residues per peptide engaged in structures – 4.4 (Fig. 4b) – is 57% higher, compared to the p2 monomeric simulation (Section 3.1). Many peptides within the aggregate remain largely unstructured, but some form well-defined and stable β-sheets, that are 5-7 residues long (Fig. 3b and Supp. Fig. S7).

We have collected some experimental data in order to corroborate our simulations. Far-UV CD spectra of p1 and p2 were recorded in order to extract the secondary structure contents of the peptides. Experimental conditions are described in sec. 2.5. Far-UV CD spectra of the peptides at a concentration of 0.1 mg/mL show that they adopt a random coil conformation with a minimum at 198 nm. Furthermore, a shoulder around 220 nm, which is a typical signature of secondary structure contents, is also observed (Fig. 5 and Supp. Fig. S8): for both p1 and p2, the far-UV CD spectra indicate the formation of transient helical (˜5%), extended (˜30%), turns (˜25%) and disordered (˜40%) conformations. A similar secondary structure profile is found at higher concentrations (5.5 mg/mL for p1 and 5.7 mg/mL for p2) as reported in Table 3. These results are consistent with the synthetic data in as far as the lower concentration may be considered a reasonable approximation for the single-monomer solution, sec. 3.1.

Size-exclusion chromatograms of both peptides show unique peaks at their respective elution volume (Supp. Fig. S9). The masses derived from MALS analysis are in agreement with the expected theoretical masses (Table 4), demonstrating that the peptides are monomeric and not in an aggregated form in solution at low concentration.

SAXS data was collected in order to probe the overall properties of the peptides in solution. The normalized Kratky representations (Supp. Fig. S10a) of p1 and p2 have no clear maximum and exhibit a monotonic increase along the momentum transfer range, which indicates that the peptides are disordered, in agreement with

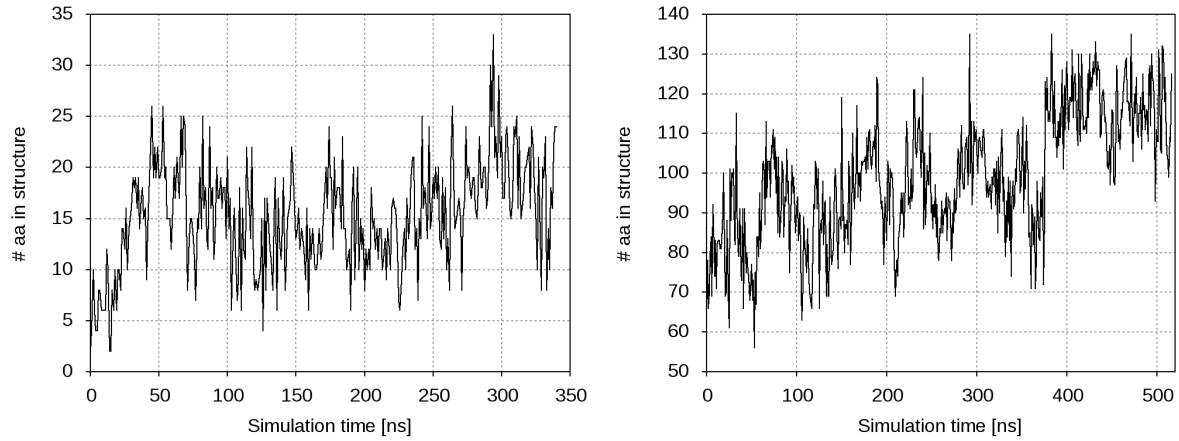

(a) *(b)*

Figure 4: Number of amino acid residues, participating in any secondary structure element in the mono-component a p1 and b p2 peptide solution simulation.

Table 3: Secondary structure contents extracted from Far-UV CD spectra of p1 and p2 at a concentration of 5.5 mg/mL. Regular (1) and distorted (2) alpha helix or beta strand, turns and unordered regions. NRMSD normalized root mean square deviation.

Peptide	Helix 1	Helix 2	Strand 1	Strand 2	Turns	Unordered	Total	NRMSD
p1	0.006	0.056	0.202	0.123	0.229	0.385	1.001	0.054
p2	0.003	0.055	0.186	0.117	0.233	0.406	1.000	0.066

Table 4: Molar mass comparison of p1 and p2 peptides. The theorical molar masses were calculated with Protparam tool from Expasy Swiss Bioinformatics Resource PortaL The experimental molar masses were determined by SEC-MALS using Light scattering chromatograms analyzes with ASTRA software (Wyatt^{TM}).

	Theoretical molar mass (kDa)	Experimental molar mass (kDa)
p1	1.17	$1.2 \pm 2.3\%$
p2	1.57	$1.5 \pm 1.2\%$

the simulation data about the small fraction of structure-participating residues in both monocomponent solutions. The SAXS curves of p1 at the 2.5 to 10 mg/mL are perfectly identical, meaning that the peptide does not present protein concentration dependence until 10 mg/mL (Supp. Fig. S10b). A slight phenomenon of repulsion is observed in solution (small decrease of the curves at low q). The SAXS curves of p2 at 2.5 and 10 mg/mL do not perfectly superimpose, exhibiting a slight aggregation which is more pronounced at 10 mg/mL. The curves difference is most likely due to the greater presence of aggregates in the more concentrated sample. In Table 5 the results of Guinier's analysis of the initial part of the curve (qR$_g$ ¡ 1.1, where q is the momentum transfer and R$_g$ is the radius of gyration) for both p1 and p2 are shown.

The size of aggregates of the p2 peptide cannot be extracted from the available data. However, SAXS data shows that p1 does not undergo aggregation process in this range of concentration, while for p2 some aggregates are observed at all investigated concentration.

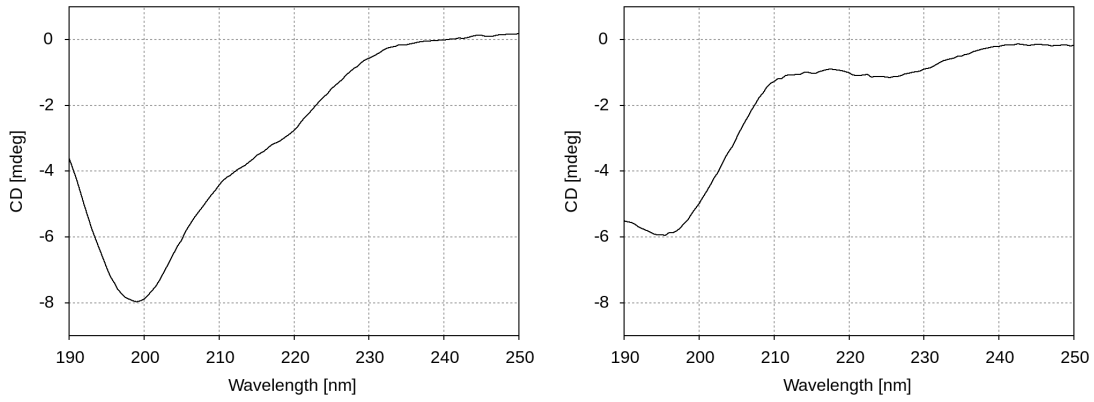

(a) *(b)*

Figure 5: Far-UV CD spectra of (A) p1 and (B) p2 at 0.1 mg/mL and 23°C.

Table 5: Radius of gyration and the respective I(0) values for p1 and p2 as obtained from the SAXS data.

	2.5 mg/mL		**10 mg/mL**	
	$\mathbf{R}_g$[Å]	I(0)	$\mathbf{R}_g$[Å]	I(0)
p1			6.64 ± 0.02	0.0075
p2	10.17 ± 0.13	0.0016	10.39 ± 0.05	0.0055

3.3 Multicomponent peptide solution

The peptides p1 and p2 investigated in this study were isolated from the lightest fraction of the *Helix aspersa* mucus [13, 24]. It is worth pointing out that the peptides are not secreted as monomers, but as part of a multicomponent mixture of peptides, carbohydrates and various other low-molecular weight compounds (acids, salts, etc.) [52]. Taking this into account, we performed an MD simulation of a mixture of the two studied peptides. The solution contained 25 p1 and 10 p2 peptides, placed randomly on a lattice with a minimal distance between the peptides of 5 nm, as well as counter-ions to neutralize the whole system. The simulation duration was 1 μs.

The peptide aggregation that was observed in the mono-component solutions simulations also takes place in this multicomponent system. The evolution of the largest-cluster size during the simulation is shown in Fig. 2 (the green line). On average, after convergence of the simulation, the largest aggregate in the mixed solution has an intermediate size with its 16 monomers when compared to the two mono-component solutions. However, this cluster contains nine of the ten hydrophobic p2 peptides in the box, so its size might be an artifact of the simulation setup.

Initially, p2 peptides form dimers and trimers. They quickly associate with p1 monomers, forming small oligomers. This process is followed by the hydrophobic-effect driven aggregation of the tri- and tetramers into a nonamer. About 50 ns later nine p2 monomers have associated into the largest cluster. In the following hundred nanoseconds the aggregate recruits a few more p1 monomers and its size stabilizes.

A representative conformation of the largest p1+p2 aggregate is shown in Fig. 6. Unsurprisingly, the nine highly hydrophobic p2 monomers (presented in pink in Fig. 6a) form a large lump that is relatively uniformly covered by seven p1 peptides (in cyan in Fig. 6a). With its hydrophobic core and hydrophilic surface the aggregate has the classical structure of a globular protein (Fig. 6b).

The aggregation-driven folding, observed in the mono-component solutions simulations, that was especially noticeable in the p2 solution is also present in the p1+p2 mixture. The number of structured amino acid residues increases steadily from about 45 to 58$\pm$9 in the last 200 ns of the simulation (Suppl. Fig. S4), primarily due to an increase in the number of residues participating in β-

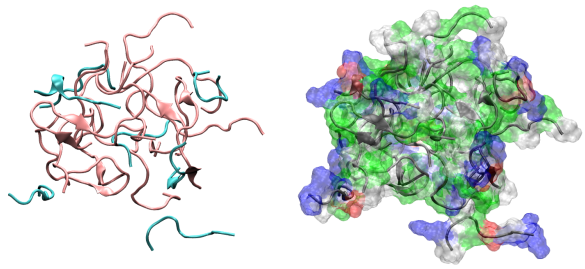

(a) (b)

Figure 6: Largest aggregates in the multicomponent p1+p2 solution simulation. a Cartoon representation according to the peptide type – p1 monomers are in cyan, p2 monomers are in pink; b Surface representation according to residue type – basic residues are in blue, acidic – red, polar – green and non-polar – white.

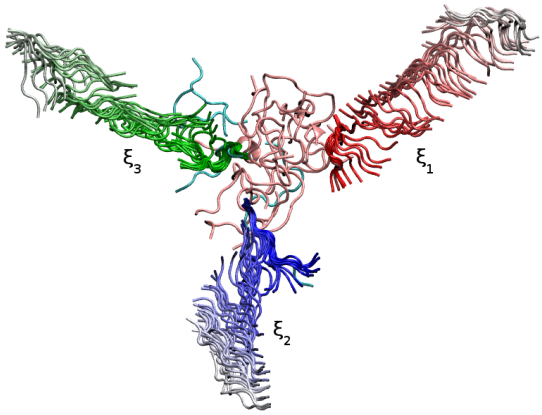

Figure 7: Peptide trajectories along the collective variables ξ_1 (blue), ξ_2 (red), and ξ_3 (green) used in the umbrella sampling simulations. The p1 peptides are coloured in cyan, and the p2 peptides are in pink.

turn and β-sheets (Suppl. Fig. S5). This more modest increase in the structure content is due to the lower number of p2 peptides in the aggregates (due to the lower total number of p2 peptides in the system) when compared to the mono-component p2 solution simulation. The structured aa residues are mainly from p2 peptides, but three of the seven p1 peptides in the aggregate also participate in relatively stable short β-sheets (Suppl. Fig. S11).

Once this large 16-mer mixed aggregate forms, it remains stable throughout the rest of the simulation. To quantitatively assess its stability, we performed US simulations. Based on the behavior of the p2 peptides in the mono-component solution simulation, we did not expect any of the highly hydrophobic p2 monomers to dissociate from the cluster. If any peptides were prone to leave the aggregate, that would be p1 peptides due to the electrostatic repulsion from other p1 monomers potentially overcoming the attraction due to the hydrophobic effect. The dissociation free energy of the most solvent exposed and hence least strongly associated to the cluster p1 monomers is an appropriate indicator for the aggregate's stability. To estimate it, the PMF was calculated along three independent collective variables ξ_1, ξ_2, ξ_3, defined as the COM distance between the respective p1 monomer and the aggregate, as represented in Fig. 7.

The respective histograms of the configurations within the US windows and the PMF along each of the three CVs are shown in Fig. 8. As is evident from the histograms, the whole range of variation of the three CVs are well explored, the windows have proper overlapping and there are no undersampled regions. The estimated from the PMFs dissociation free energies are respectively $G^1_{dissoc} = 15.3 \pm 0.6$ kcal/mol, $G^2_{dissoc} = 24 \pm 0.5$ kcal/mol, and $G^3_{dissoc} = 17.1 \pm 0.9$ kcal/mol. These are fairly high values with respect to the thermal fluctuation in the system ($k_BT \sim 0.6$kcal/mol at T=300K). Therefore, the mixed p1+p2 aggregates are very stable and their spontaneous depolymerization is not expected because of the high energetic barrier for it to take place.

4 Discussion

The leading advantage of AMPs over conventional antibiotics is their high cellular selectivity due to their cationic and amphiphilic nature. The AMPs cationic nature allows them to bind electrostatically to the negatively charged lipids in the bacterial membranes, while their amphiphilic character helps them to get inserted into the amphiphilic lipid bilayer, inducing pores or translocating into the intracellular space [30]. This mechanism appears to be well understood, but many aspects remain unclear, including the AMPs' behavior in solution, in which they are secreted, transported, and exert hemolytic activity.

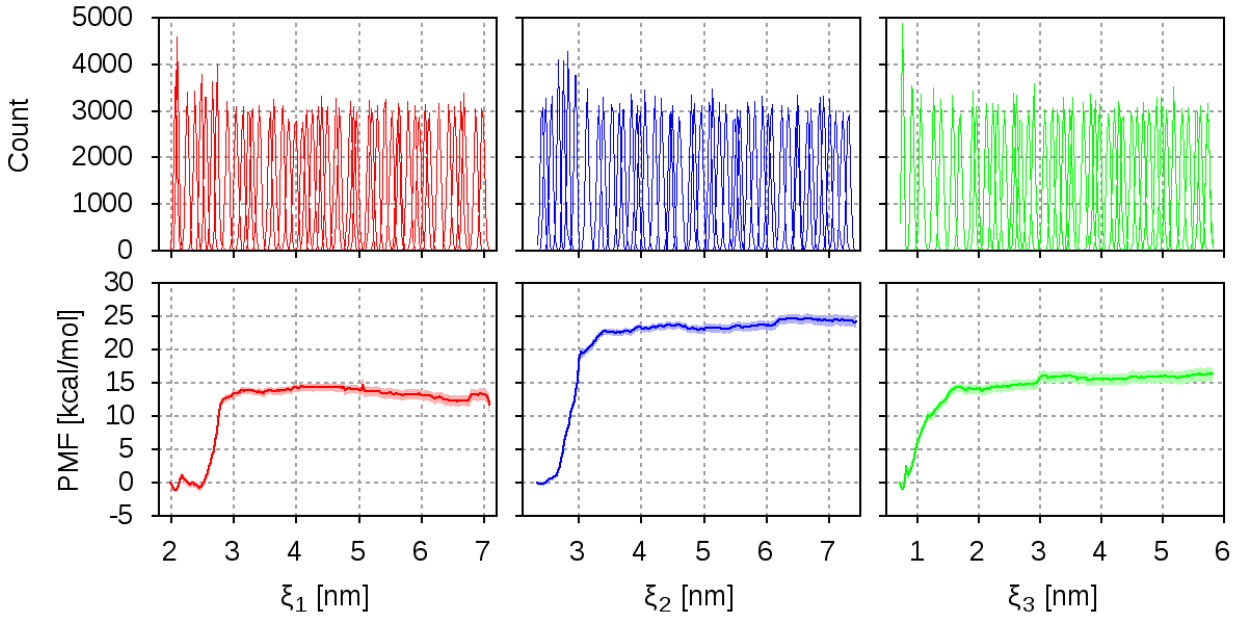

Figure 8: Histograms (upper panel) and potential of mean force (lower panel) for the three umbrella sampling simulations.

Currently, most MD studies of AMPs use as initial configurations peptide monomers near the bacterial bilayer (i.e., starting with S-state). However, AMPs are not released as monomers in solution, but are part of multicomponent secretory fluids, exhibiting certain biological activity. The snail mucus is composed of a large variety of peptides, carbohydrates, salts and other low-molecular weight compounds [52]. In [53, 13, 14] it was shown that the lightest peptide fraction of the mucus of the garden snail *Helix aspersa* with molecular weight 1–10kDa displayed antimicrobial activity.

Even though cationic AMPs are the most common AMPs, neutral and even anionic AMPs do exist. While according to the AMP database [1, 54] there are over 2893 cationic AMP entries, at least 190 neutral and 196 anionic peptides have been identified so far. There is experimental evidence that a positive charge is not required for the antimicrobial activity of some AMPs [8]. In fact, in some fungal species more than 70% of the putative CS$\alpha\beta$ defensins carry net negative or neutral charges under pH 7.0 [55]. A large amount of the identified in the *Helix aspersa* mucus antimicrobial peptides are not cationic [53, 13, 14, 24]. This data raises the question of the role that the non-cationic peptides play in the antimicrobial secretions in different species.

This motivated us to explore the interaction of multiple peptides in solution, modelling their behaviour in the antimicrobial fluids (in this case – the snail mucus), right after secretion and prior to their interaction with the pathogenic membranes. Selecting a putative neutral AMP as a test sample, we also aimed at addressing the role of the neutral AMPs in the antimicrobial action of the mixtures and their interaction with cationic peptides.

We have previously demonstrated on the example of magainin and bombinin H2 that the secondary structure of monomeric AMPs in solution is not stable and they usually adopt a conformation that is not the most favorable for exerting their biological activity [41, 42]. Other linear AMPs were also shown to self-associate in water solution [36, 42] in large nano-sized clusters. In recent years, more and more studies have focused on self-assembling AMPs, which form nanostructures that can

exhibit distinct physicochemical properties from their single molecular components and extend their applications in many fields. The resultant AMPs systems are fully biocompatible and biodegradable and demonstrate high antimicrobial activity without compromising biological safety over mammalian cells [50, 49, 46]. While this is not necessarily true for all AMPs, amphiphilic peptides are prone to self-assembly and able to form micelles, vesicles, fibrils, and nanotubes, depending on peptide length, distribution of hydrophobicity and charge, nature of charged groups and counterions [10, 9, 48]. In addition, we previously demonstrated that this aggregation process drives a significant portion of the peptide chains to permanently transition to their biologically active conformation prior to attacking the bacterial membrane by providing the necessary amphypathic environment mimicking the membrane–solvent interface [42].

Here, we used two putative AMPs isolated from the lightest fraction of the mucus of *Helix aspersa* in order to perform an *in silico* study of a model multicomponent AMP mixture. The peptide monomers in both the mono- and the multicomponent solutions quickly (in the nanosecond range) start to self-associate into clusters. Aggregation allows for an increase in the number of inter-peptide hydrogen bonds, which promotes the formation of new and stabilizes already formed secondary structure elements. The size and properties of the aggregates depend on the composition of the solution, but in general, similarly to globular proteins, they consist of a non-polar hydrophobic core and exposed to the solvent charged and polar residues.

In addition, it should be noted, that the CD spectra were taken in a BisTris buffer known for its pronounced aggregation-suppression behaviour. As proposed in [42], in the process of cluster formation, aggregation-driven folding that substantially increases not only the peptides' local concentration, but also the fraction of peptides embarking on the target membrane in a biologically functional conformation takes place. In the BisTris buffer, this process is impeded, which, in conjunction with the gradual crowding provoked by the concentration increase, might even lead to a decrease in the detected structured content.

It is not clear which components of the snail mucus are responsible for its antimicrobial activity. In the model multi-component system, the neutral p2 peptide monomers form the hydrophobic core of the cluster, while the cationic p1 monomers remain solvent-exposed on its surface. There are two possible scenarios for the role of the non-cationic peptides. In the first one, the non-cationic peptides may not directly possess antibacterial activity. In this case our results suggest that they act as a system for the cationic peptides, delivering a high local concentration of them to the pathogenic membrane. In the second scenario, the non-cationic peptides might also have antimicrobial properties. It is highly unlikely that an anionic or even uncharged hydrophobic peptide would spontaneously target negatively charged pathogenic membranes. So we hypothesize that in this case they use the cationic peptide coating of the clusters as a navigation system that is electrostatically attracted by the negatively charged phospholipids in the bacterial membranes. Once delivered to the bilayer, the hydrophobic effect drives the interaction between the non-cationic peptides and the hydrophobic tails of the lipids.

Regardless of the scenario, we propose that the so-formed structures provide the perfect transport system – locking the hydrophobic uncharged residues in the core of the cluster prevents the interaction with the eukaryotic membranes with lower surface charge density, and positioning the charged residues on the cluster surface enables for electrostatic interaction with the bacterial surface (S-state). In addition, the peptide folding, promoted by the amphiphilic structure in the aggregates, allows for a sufficiently high local concentration of AMPs to be delivered to the target membrane in a functionally active conformation.

Acknowledgments

This work is partly supported by the Bulgarian Science Fund under Grant KP-06-OPR 03-10/2018 (P.P., N.I., E.L., and L.L.). The CBS is a member of the French Infrastructure for Integrated Structural Biology (FRISBI) supported by the French National Research Agency (ANR-10-INSB-05). N.S. acknowledges the support of the ANR GPCteR (ANR-17- CE11-0022-01) and the Labex EpiGenMed (ANR-10-LABX-12-01).

Computational resources were provided by the BioSim HPC Cluster at the Faculty of Physics at Sofia University "St. Kl. Ohridski", Sofia (Bulgaria) and by CI TASK (Centre of Informatics – Tricity Academic Supercomputer

& networK), Gdansk (Poland). We thank the synchrotron facility SOLEIL (St. Aubin) for allocating regular beam time (Block Allocation Group, proposal No. 20201085) and its dedicated staff for technical help with the beamline SWING. We thank the DISCO beamline and its dedicated staff for the acquisition of CD data on their in-house time. We thank the Biophysical Characterization facility of the Biocampus PIBBPS platform. We also thank P. Dolashka and L. Velkova for the discussions and B. Pavlov for the help in data curation.

Abbreviations

The following abbreviations are used in this manuscript:

AMP	Antimicrobial peptide
MD	Molecular dynamics
PMF	Potential of mean force
SMD	Steered molecular dynamics
US	Umbrella sampling
WHAM	Weighted histogram analysis method

SUPPLEMENTARY MATERIALS

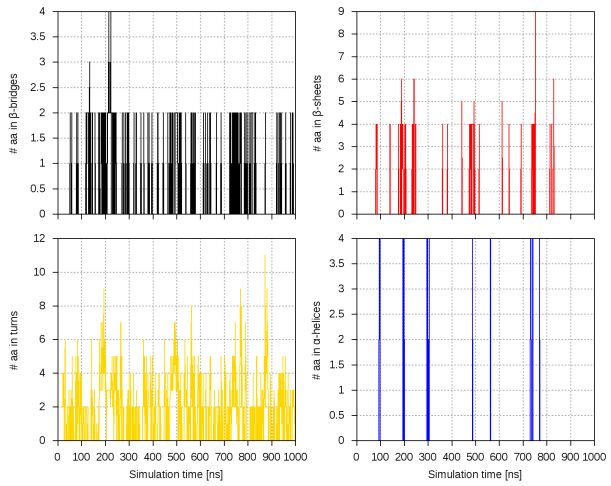

*Figure: **S1.** Number of amino acid residues in various types of secondary structures in the p2 monomer in water simulation.*

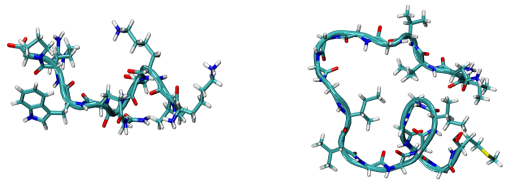

*Figure: **S2.** Peptide conformations ised as input structures for the subsequent simulations: (a) for p1; (b) for p2.*

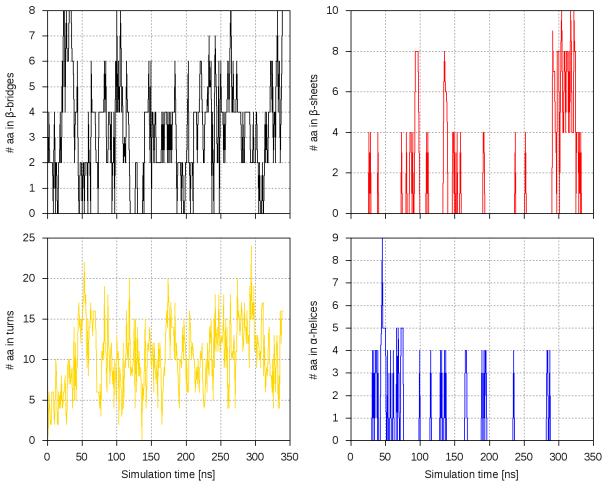

*Figure: **S3.** Number of amino acid residues in various types of secondary structures in the p1 solution simulation.*

References

[1] Antimicrobial peptide database.

[2] Mark James Abraham, Teemu Murtola, Roland Schulz, Szilárd Páll, Jeremy C. Smith, Berk Hess, and Erik Lindahl. Gromacs: High performance molecular simulations through multi-level parallelism from laptops to supercomputers. *SoftwareX*, 1-2:19 – 25, 2015.

[3] J.M. Ageitos, A. Sánchez-Pérez, P. Calo-Mata, and T.G. Villa. Antimicrobial peptides (amps): Ancient compounds that represent novel weapons in the fight against bacteria. *Biochemical Pharmacology*, 133:117 – 138, 2017.

[4] CE Blanchet and DI Svergun. Small-angle x-ray scattering on biological macromolecules and nanocomposites in

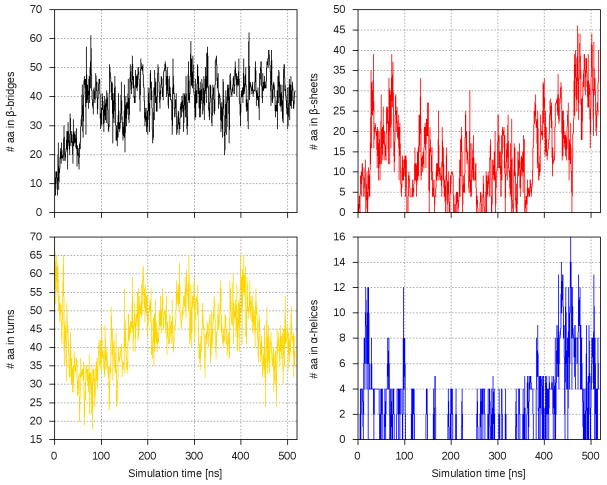

*Figure: **S4.** Number of amino acid residues in various types of secondary structures in the p2 solution simulation.*

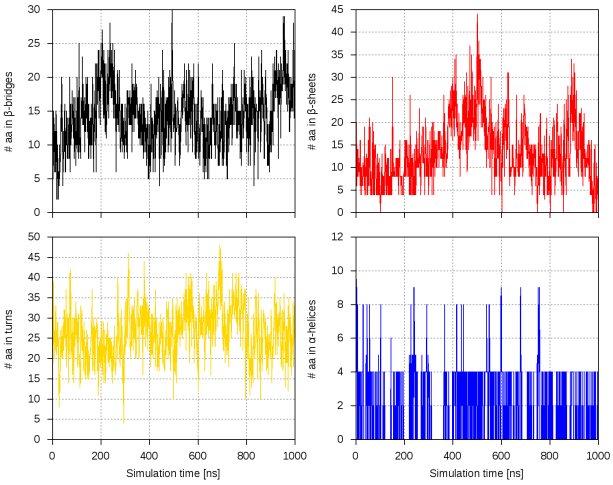

*Figure: **S6.** Number of amino acid residues in various types of secondary structures in the mixed p1+p2 solution simulation.*

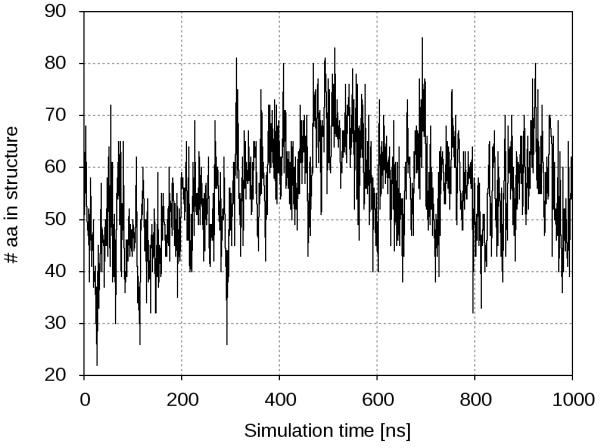

*Figure: **S5.** Number of amino acid residues, participating in any secondary structure element in the multicomponent p1+p2 solution simulation.*

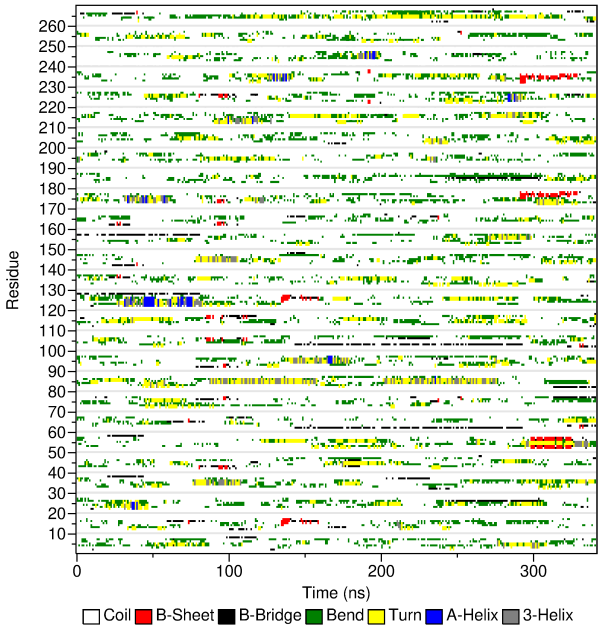

*Figure: **S7.** Secondary structure of the peptides in the p1 monocomponent solution simulation.*

solution. *Annual Review of Physical Chemistry*, 64:37–54, 2013.

[5] Hans G. Boman. Peptide antibiotics and their role in innate immunity. *Annual Review of Immunology*, 13(1):61–92, 1995.

[6] Giovanni Bussi, Davide Donadio, and Michele Parrinello.

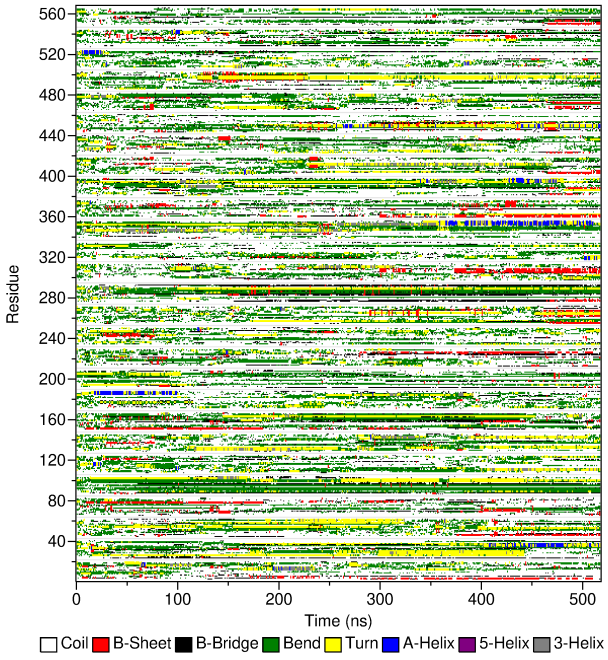

*Figure: **S8.** Secondary structure of the peptides in the p2 monocomponent solution simulation.*

Canonical sampling through velocity rescaling. *The Journal of chemical physics*, 126(1):014101, 2007.

[7] Ana Maria Carmona-Ribeiro and Letícia Dias de Melo Carrasco. Cationic antimicrobial polymers and their assemblies. *International Journal of Molecular Sciences*, 14:9906–9946, 2013.

[8] Gabriela Contreras, Markus Santhosh Braun, Holger Schäfer, and Michael Wink. Recombinant afusinc, an anionic fungal cs$\alpha\beta$ defensin from aspergillus fumigatus, exhibits antimicrobial activity against gram-positive bacteria. *PLOS ONE*, 13(10):1–12, 2018.

[9] Honggang Cui, Matthew J. Webber, and Samuel I. Stupp. Self-assembly of peptide amphiphiles: From molecules to nanostructures to biomaterials. *Peptide Science*, 94(1):1–18, 2010.

[10] A Dehsorkhi, V Castelletto, and I.W. Hamley. Self-assembling amphiphilic peptides. *Journal of Peptide Science*, 20(7):453–67, 2014.

[11] Pavlina Dolashka, Aleksander Dolashki, Wolfgang Voelter, Jozef Van Beeumen, and Stefan Stevanovic. Antimicrobial activity of peptides from the hemolymph of helix lucorum snails. *International Journal of Current Microbiology and Applied Sciences*, 4(4):1061–1071, 2015.

[12] Pavlina Dolashka, Vesela Moshtanska, Valika Borisova, Aleksander Dolashki, Stefan Stevanovic, Tzvetan Dimanov, and Wolfgang Voelter. Antimicrobial proline-rich peptides from the hemolymph of marine snail rapana venosa. *Peptides*, 32(7):1477 – 1483, 2011.

[13] A. Dolashki, A. Nissimova, E. Daskalova, L. Velkova, Y. Topalova, P. Hristova, P. Traldi, W. Voelter, and P. Dolashka. Structure and antibacterial activity of isolated peptides from the mucus of garden snail cornu aspersum. *Bulgarian Chemical Communications*, 50(C):195 – 200, 2018.

[14] A Dolashki, L Velkova, E Daskalova, N Zheleva, Y Topalova, V Atanasov, W Voelter, and P Dolashka. Antimicrobial activities of different fractions from mucus of the garden snail cornu aspersum. *Biomedicines*, 8(9):315, 2020.

[15] Ulrich Essmann, Lalith Perera, Max L Berkowitz, Tom Darden, Hsing Lee, and Lee G Pedersen. A smooth particle mesh ewald method. *The Journal of Chemical Physics*, 103(19):8577–8593, 1995.

[16] Christopher D. Fjell, Jan A. Hiss, Robert E. W. Hancock, and Gisbert Schneider. Designing antimicrobial peptides: form follows function. *Nature Reviews Drug Discovery*, 11:37–51, 2012.

[17] F Guilhelmelli, N Vilela, P Albuquerque, L Derengowski, I Silva-Pereira, and C Kyaw. Antimicrobial development challenges: the various mechanisms of action of antimicrobial peptides and of bacterial resistance. *Frontiers in Microbiology*, 4:353, 2013.

[18] Robert E W Hancock and Hans-Georg Sahl. Antimicrobial and host-defense peptides as new anti-infective therapeutic strategies. *Nature Biotechnology*, 24:1551–1557, 2006.

[19] E. F. Haney, S. C. Mansour, and R. E. Hancock. Antimicrobial peptides: An introduction. *Methods in molecular biology*, 1548:3–22, 2017.

[20] Berk Hess. P-lincs: A parallel linear constraint solver for molecular simulation. *Journal of Chemical Theory and Computation*, 4(1):116–122, 2008.

[21] R.W Hockney, S.P Goel, and J.W Eastwood. Quiet high-resolution computer models of a plasma. *Journal of Computational Physics*, 14(2):148 – 158, 1974.

[22] Jochen S. Hub, Bert L. de Groot, and David van der Spoel. g_wham—a free weighted histogram analysis implementation including robust error and autocorrelation estimates. *Journal of Chemical Theory and Computation*, 6(12):3713–3720, 2010.

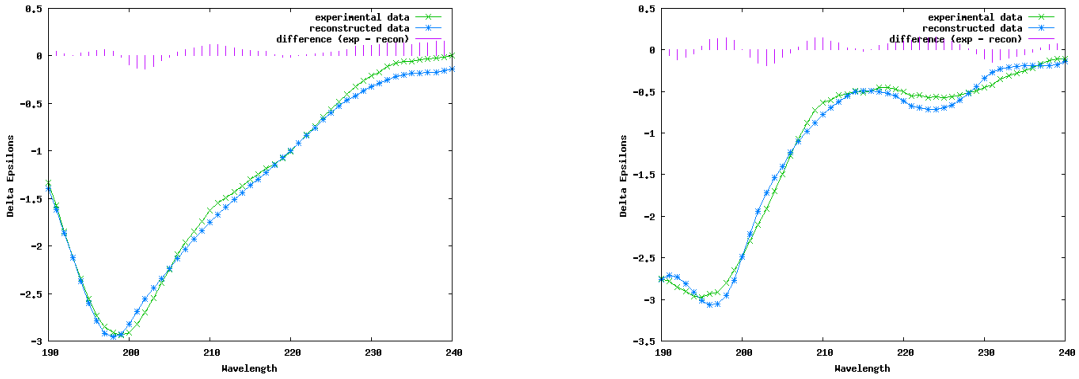

*Figure: **S9.** Far-UV CD spectra of (a) p1 and (b) p2 at 5.5 mg//mL, resp. 5.7 mg/mL. Experimental data is represented in green, reconstructed data in blue and the difference – in pink. The normalized root mean square deviation (NRMSD) values are respectively of 0.054 and 0.066.*

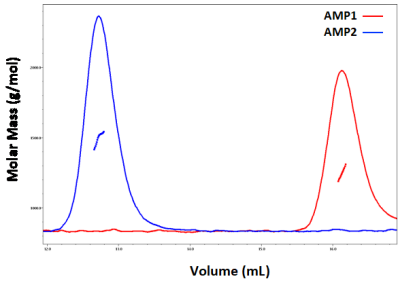

*Figure: **S10.** Light scattering chromatogram of p1 (red) and p2 (blue). The molar mass is determined by MALS and the molar mass variation of each peptide is represented by a solid line inside the corresponding chromatogram peak. SEC-MALS data has been measured at 25 °C.*

[23] William Humphrey, Andrew Dalke, and Klaus Schulten. VMD – Visual Molecular Dynamics. *Journal of Molecular Graphics*, 14:33–38, 1996.

[24] N Ilieva, P. Petkov, E. Lilkova, T. Lazarova, A. Dolashki, L. Velkova, P. Dolashka, and L. Litov. In silico study on the structure of novel natural bioactive peptides. In *Large-Scale Scientic Computing. LSSC 2019.*, volume 11958 of *Lecture Notes in Computer Science*, pages 332–339. Springer, 2020.

[25] Håvard Jenssen, Pamela Hamill, and Robert E. W. Hancock. Peptide antimicrobial agents. *Clinical Microbiology Reviews*, 19(3):491–511, 2006.

[26] Wolfgang Kabsch and Christian Sander. Dictionary of protein secondary structure: Pattern recognition of hydrogen-bonded and geometrical features. *Biopolymers*, 22(12):2577–2637, 1983.

[27] Shankar Kumar, John M. Rosenberg, Djamal Bouzida, Robert H. Swendsen, and Peter A. Kollman. The weighted histogram analysis method for free-energy calculations on biomolecules. i. the method. *Journal of Computational Chemistry*, 13(8):1011–1021, 1992.

[28] Justin A. Lemkul and David R. Bevan. Assessing the stability of alzheimer's amyloid protofibrils using molecular dynamics. *The Journal of Physical Chemistry B*, 114(4):1652–1660, 2010.

[29] H. Li, M.G. Parisi, N. Parrinello, M. Cammarata, and P. Roch. Molluscan antimicrobial peptides, a review from activity-based evidences to computer-assisted sequences. *Invertebrate Survival Journal*, 8:85–97, 2011.

[30] Shuqin Li, Yajie Wang, Zihan Xue, Yanan Jia, Ruilin Li, Chengwei He, and Haixia Chen. The structure-mechanism relationship and mode of actions of antimicrobial peptides: A review. *Trends in Food Science & Technology*, 109:103–115, 2021.

[31] Simon C. Lovell, Ian W. Davis, W. Bryan Arendall III, Paul I. W. de Bakker, J. Michael Word, Michael G. Prisant, Jane S. Richardson, and David C. Richardson. Structure

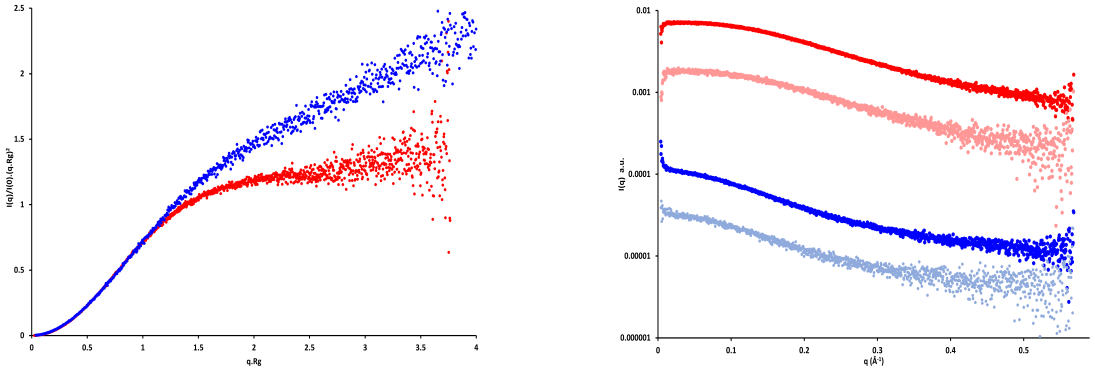

(a) *(b)*

Figure: ***S11.*** *(a) Normalized Kratky plot of p1 (blue) and p2 (red) at 10 mg/mL displaying that there is no return to the baseline as it would be the case for a fully structured peptide; (b) SAXS curves of p1 at 2.5 mg/mL (light blue) and at 10 mg/mL (blue), p2 at 2.5 mg/mL (light red) and 10 mg/mL (red). For better visualization of SAXS curves, the intensities of p2 SAXS curves have been divided by 50.*

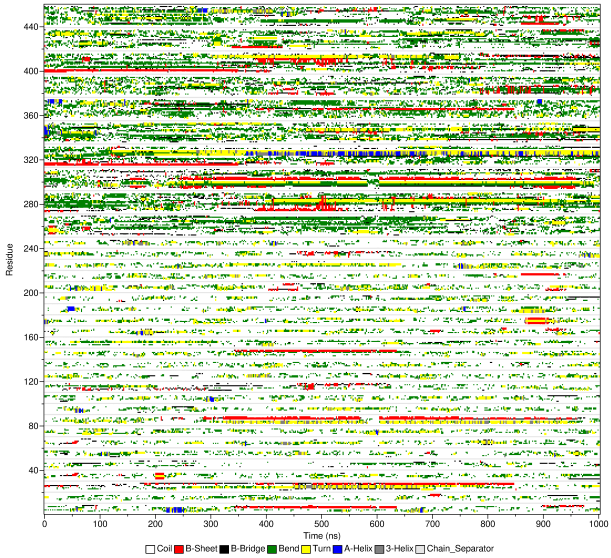

Figure: ***S12.*** *Secondary structure of the peptides in the p1+p2 mixed solution simulation.*

validation by cα geometry: ϕ, ψ and cβ deviation. *Proteins: Structure, Function, and Bioinformatics*, 50(3):437–450, 2003.

[32] H. X. Luong, T. T. Thanh, and T. H. Tran. Antimicrobial peptides - advances in development of therapeutic applications. *Life Sciences*, 260:118407, 2020.

[33] A. D. MacKerell, D. Bashford, M. Bellott, R. L. Dunbrack, J. D. Evanseck, M. J. Field, S. Fischer, J. Gao, H. Guo, S. Ha, D. Joseph-McCarthy, L. Kuchnir, K. Kuczera, F. T. K. Lau, C. Mattos, S. Michnick, T. Ngo, D. T. Nguyen, B. Prodhom, W. E. Reiher, B. Roux, M. Schlenkrich, J. C. Smith, R. Stote, J. Straub, M. Watanabe, J. Wiórkiewicz-Kuczera, D. Yin, and M. Karplus. All-atom empirical potential for molecular modeling and dynamics studies of proteins. *The Journal of Physical Chemistry B*, 102(18):3586–3616, 1998.

[34] Alexander D. Mackerell Jr., Michael Feig, and Charles L. Brooks III. Extending the treatment of backbone energetics in protein force fields: Limitations of gas-phase quantum mechanics in reproducing protein conformational distributions in molecular dynamics simulations. *Journal of Computational Chemistry*, 25(11):1400–1415, 2004.

[35] Margit Mahlapuu, Joakim Håkansson, Lovisa Ringstad, and Camilla Björn. Antimicrobial peptides: An emerging category of therapeutic agents. *Frontiers in Cellular and Infection Microbiology*, 6:194, 2016.

[36] R. Marinova, P. Petkov, N. Ilieva, E. Lilkova, and Litov L. Molecular dynamics study of the solution behaviour of antimicrobial peptide indolicidin. In *Advanced Computing in Industrial Mathematics. BGSIAM 2017.*, volume 793 of *Studies in Computational Intelligence*, pages 257–265. Springer, 2019.

[37] AJ Miles, SG Ramalli, and BA Wallace. Dichroweb, a website for calculating protein secondary structure from circular dichroism spectroscopic data. *Protein Science*, 31(1):37–46, 2022.

[38] K. Pärn, E. Eriste, and Ü. Langel. The antimicrobial and antiviral applications of cell-penetrating peptides. *Methods in molecular biology*, 1324:223–245, 2015.

[39] M. Parrinello and A. Rahman. Crystal structure and pair potentials: A molecular-dynamics study. *Physical Review Letters*, 45:1196, 1980.

[40] M. Parrinello and A. Rahman. Polymorphic transitions in single crystals: A new molecular dynamics method. *Journal of Applied Physics*, 52:7182, 1981.

[41] P. Petkov, R. Marinova, V. Kochev, N. Ilieva, E. Lilkova, and L. Litov. Computational study of solution behavior of magainin 2 monomers. *Journal of Biomolecular Structure and Dynamics*, 37(5):1231–1240, 2019.

[42] Peicho Petkov, Elena Lilkova, Nevena Ilieva, and Leandar Litov. Self-association of antimicrobial peptides: A molecular dynamics simulation study on bombinin. *International Journal of Molecular Sciences*, 20(21):5450, 2019.

[43] S. J. Pitt, M. A. Graham, C. G. Dedi, P. M. Taylor-Harris, and A. Gunn. Antimicrobial properties of mucus from the brown garden snail helix aspersa. *British journal of biomedical science*, 72(4):174–181, 2015.

[44] SW Provencher and J Glockner. Estimation of globular protein secondary structure from circular dichroism. *Biochemistry*, 20:33–37, 1981.

[45] Durba Sengupta, Hari Leontiadou, Alan E. Mark, and Siewert-Jan Marrink. Toroidal pores formed by antimicrobial peptides show significant disorder. *Biochimica et Biophysica Acta*, 1778:2308–2317, 2008.

[46] Zhiwei Shen, Zhen Guo, Limin Zhou, Yujiao Wang, Jinjin Zhang, Jun Hu, and Yi Zhang. Biomembrane induced in situ self-assembly of peptide with enhanced antimicrobial activity. *Biomaterials Science*, 8(7):2031–2039, 2020.

[47] N Sreerama and RW Woody. Estimation of protein secondary structure from cd spectra: Comparison of contin, selcon and cdsstr methods with an expanded reference set. *Anales in Biochemistry*, 287(2):252–260, 2000.

[48] L. Sun, C. Zheng, and T. J. Webster. Self-assembled peptide nanomaterials for biomedical applications: promises and pitfalls. *International journal of nanomedicine*, 12:73–86, 2016.

[49] M. C. Teixeira, C. Carbone, M. C. Sousa, M. Espina, M. L. Garcia, E. Sanchez-Lopez, and E. B. Souto. Nanomedicines for the delivery of antimicrobial peptides (amps). *Nanomaterials*, 10(3):560, 2020.

[50] Chaitanya K. Thota, Allison A. Berger, Björn Harms, Maria Seidel, Christoph Böttcher, Hans von Berlepsch, Chaunxiong Xie, Roderich Süssmuth, Christian Roth, and Beate Koksch. Short self-assembling cationic antimicrobial peptide mimetics based on a 3,5-diaminobenzoic acid scaffold. *Peptide Science*, 112(1):e24130, 2020.

[51] A Thureau, P Roblin, and J Pérez. Biosaxs on the swing beamline at synchrotron soleil. *Journal of Applied Crystallography*, 54:1698–1710, 2021.

[52] C. Trapella, R. Rizzo, S. Gallo, A. Alogna, D. Bortolotti, F. Casciano, G. Zauli, P. Secchiero, and R. Voltan. Helixcomplex snail mucus exhibits pro-survival, proliferative and pro-migration effects on mammalian fibroblasts. *Scientific reports*, 8(1):17665, 2018.

[53] L. Velkova, A. Nissimova, A. Dolashki, E. Daskalova, P. Dolashka, and Y. Topalova. Glycine-rich peptides from cornu aspersum snail with antibacterial activity. *Bulgarian Chemical Communications*, 50:169 – 175, 2018.

[54] Guangshun Wang, Xia Li, and Zhe Wang. APD3: the antimicrobial peptide database as a tool for research and education. *Nucleic Acids Research*, 44(D1):D1087–D1093, 2015.

[55] Y. Wu, B. Gao, and S. Zhu. New fungal defensin-like peptides provide evidence for fold change of proteins in evolution. *Bioscience reports*, 37(1):BSR20160438, 2017.

[56] N.Y. Yount and M.R. Yeaman. Emerging themes and therapeutic prospects for anti-infective peptides. *Annual Review of Pharmacology and Toxicology*, 52:337–360, 2012.

[57] M. Zasloff. Antimicrobial peptides of multicellular organisms. *Nature*, 415:389–395, 2002.

[58] J Zhong, W Wang, X Yang, X Yan, and R Liu. A novel cysteine-rich antimicrobial peptide from the mucus of the snail of achatina fulica. *Peptides*, 39:1–5, 2013.

[59] Jun Zhuang, Christopher J Coates, Hongtao Zhu, Ping Zhu, Zujian Wu, and Lianhui Xie. Identification of candidate antimicrobial peptides derived from abalone hemocyanin. *Developmental & Comparative Immunology*, 49(1):96–102, 2015.